DOI: 10.1002/chem.200700293

Synthesis, Structure, and Electrochemical Properties of Sterically Protected Molybdenum Trihydride Redox Pairs: A Paramagnetic "Stretched" Dihydrogen Complex?

Miguel Baya,[a] Jennifer Houghton,[a] Jean-Claude Daran,[a] Rinaldo Poli,*[a] Louise Male,[b] Alberto Albinati,[b] and Matthias Gutman[c]

Abstract: Complexes [MoCp$^{\#}$(PMe$_3$)$_2$H$_3$] (Cp$^{\#}$ = 1,2,4-C$_5$H$_2$*t*Bu$_3$, **2a**; C$_5$H*i*Pr$_4$, **2b**) have been synthesized from the corresponding compounds [MoCp$^{\#}$Cl$_4$] (**1a**, **1b**) and fully characterized, including by X-ray crystallography and by a neutron diffraction study for **2a**. Protonation of **2a** led to complex [Mo(1,2,4-C$_5$H$_2$*t*Bu$_3$)(PMe$_3$)$_2$H$_4$]$^+$ (**3a**) in THF and to [Mo(1,2,4-C$_5$H$_2$*t*Bu$_3$)(PMe$_3$)$_2$(MeCN)H$_2$]$^+$ (**4a**) in MeCN. Complex **4b** analogously derives from protonation of **2b** in MeCN, whereas the tetrahydride complex **3b** is unstable. One-electron oxidation of **2a** and **2b** by [FeCp$_2$]PF$_6$ produces the EPR-active 17-electron complexes **2a**$^+$ and **2b**$^+$. The former is thermally more stable than the latter and could be crystallographically characterized as the PF$_6^-$ salt by X-ray diffraction, providing evidence for the presence of a stretched dihydrogen ligand (H···H = 1.36(6) Å). Controlled thermal decomposition of **2a**$^+$ yielded the product of H$_2$ elimination, the 15-electron monohydride complex [Mo(1,2,4-C$_5$H$_2$*t*Bu$_3$)(PMe$_3$)$_2$H]PF$_6$ (**5a**), which was characterized by X-ray crystallography and by EPR spectroscopy at liquid He temperature. The compound establishes an equilibrium with the solvent adduct in THF. An electrochemical study by cyclic voltammetry provides further evidence for a rapid H$_2$ elimination process from the 17-electron complexes. In contrast to the previously investigated [MoCp*(dppe)H$_3$]$^+$ system (dppe = 1,2-bis(diphenylphosphino)ethane; Cp* = pentamethylcyclopentadienyl), the decomposition of **2a**$^+$ by H$_2$ substitution with a solvent molecule appears to follow a dissociative pathway in MeCN.

Keywords: cyclopentadienyl ligands • dihydrogen elimination • hydride ligands • magnetic properties • molybdenum • neutron diffraction

Introduction

Hydride complexes have paramount importance in light of their implication in a variety of catalytic processes and as models of biological functions such as hydrogenase and nitrogenase.[1–6] Because of the strong covalent nature of the M−H σ bond and the absence of additional orbital interactions (i.e. of π type), they are usually stable only in a closed-shell configuration, in contrast to the open-shell configuration that produces reactive compounds. An interesting subclass of open-shell hydride complexes are those with an odd-electron (mostly 17-electron) configuration, characterized by paramagnetism. These complexes have generally been accessed by one-electron oxidation of stable diamagnetic precursors. In most cases, they decompose by deprotonation,[7] disproportionation,[8] dihydrogen reductive elimination (for complexes containing at least two hydride ligands),[9] atom transfer,[10] and other pathways.[11] This multitude of available reaction pathways complicates their poten-

---

[a] Dr. M. Baya, Dr. J. Houghton, Dr. J.-C. Daran, Prof. R. Poli
Laboratoire de Chimie de Coordination
UPR CNRS 8241 liée par convention à l'Université Paul Sabatier et à l'Institut National Polytechnique de Toulouse
205 Route de Narbonne, 31077 Toulouse Cedex (France)
Fax: (+33) 561-553-003
E-mail: poli@lcc-toulouse.fr

[b] Dr. L. Male, Prof. A. Albinati
Department of Structural Chemistry (DCSSI)
Università di Milano, Via G. Venezian 21
20133 Milano (Italy)

[c] Dr. M. Gutman
Rutherford Appleton Laboratory, ISIS Facility
Chilton (Didcot) OX11 0QX (UK)

Supporting information for this article is available on the WWW under http://www.chemeurj.org/ or from the author. It contains figures showing the structure of **2a** from the neutron diffraction experiment, the variable-temperature ^{31}P{^{1}H} experiment for compound **2b**, and a variety of cyclic voltammograms for **2a** and **2b** at variable scan speed in MeCN and THF.

tial application, for instance in electrocatalysis. It is therefore useful to investigate in greater detail how the various pathways depend on the reaction conditions (e.g. solvent, available substrates) and molecular parameters (e.g. stereoelectronic properties of the ligand environment). For this purpose, it is necessary to develop more stable systems. We have learned from previous investigations[9,12–16] that all decomposition pathways are disfavored by both a stronger electron-donating and more sterically-protecting ligand environment.

The oxidation of [MoCp*(dppe)H_3] (dppe = 1,2-bis(diphenylphosphino)ethane, $Ph_2PCH_2CH_2PPh_2$; Cp* = pentamethylcyclopentadienyl) was studied in the greatest detail.[9,12,16] It leads to the paramagnetic complex [MoCp*(dppe)H_3]$^+$, which is stable at low temperatures and was characterized in situ by EPR spectroscopy. The detailed investigation of its decomposition at room temperature enabled us to quantify the relative rates of deprotonation (by the residual neutral precursor), disproportionation, and H_2 elimination in various solvents.[9,16] This was the first reported example in which H_2 oxidatively induced reductive elimination could be unambiguously demonstrated and distinguished from other decomposition pathways. Oxidation of a polyhydride complex [MH_n] is expected to favor its rearrangement to a nonclassical isomer, [$MH_{n-2}(H_2)$]$^+$,[17,18] but the multitude of decomposition pathways, all possibly leading to H_2 evolution,[19] have previously made the identification of the H_2 elimination pathway uncertain.[17,20] For this specific trihydrido molybdenum complex, all three decomposition pathways were shown to occur via the nonclassical intermediate [MoCp*(dppe)H(H_2)]$^+$, although theoretical calculations and circumstantial evidence indicates that the oxidized complex adopts a classical structure. Since the nonclassical tautomer is energetically less accessible for the related tungsten system, complex [WCp*(dppe)H_3]$^+$ turned out to be sufficiently stable to be isolated and crystallographically characterized.[9]

In this contribution, we report the synthesis and investigations into new molybdenum systems, isoelectronic with [MoCp*(dppe)H_3], that contain an even more strongly donating and sterically encumbering coordination sphere. We used the two highly substituted cyclopentadienyl rings, $C_5H\textit{i}Pr_4$ and 1,2,4-$C_5H_2\textit{t}Bu_3$, in place of Cp* and two PMe_3 ligands in place of bidentate dppe. Notable results of this investigation have been the isolation and structural characterization of the 17-electron oxidation product, [Mo(1,2,4-$C_5H_2\textit{t}Bu_3$)(PMe_3)$_2H_3$]$^+$, and the observation of its subsequent H_2 elimination process leading to the 15-electron monohydride derivative, [Mo(1,2,4-$C_5H_2\textit{t}Bu_3$)(PMe_3)$_2$H]$^+$, which was also structurally characterized. Some aspects of this investigation have been recently communicated.[21] While those preliminary results will be reported again here in fuller details, stronger emphasis will be placed on complementary investigations that have not previously been described.

Results and Discussion

Synthesis and characterization of the diamagnetic trihydride complexes [MoCp$^\#$(PMe_3)$_2H_3$] (Cp$^\#$ = 1,2,4-$C_5H_2\textit{t}Bu_3$, 2a; $C_5H\textit{i}Pr_4$, 2b): Adaptation of Schrock's [MoCp*Cl_4] synthetic procedure[22,23] to the bulkier Cp$^\#$ analogues (Cp$^\#$ = 1,2,4-$C_5H_2\textit{t}Bu_3$, **a**, and $C_5H\textit{i}Pr_4$, **b**) yielded the corresponding [MoCp$^\#Cl_4$] derivatives **1a** and **1b** in good yields, see Scheme 1. Subsequent reaction of these compounds with $LiAlH_4$ in the presence of more than two equivalents of PMe_3, followed by methanolysis and crystallization from diethyl ether, yielded the corresponding trihydride derivatives, [MoCp$^\#$(PMe_3)$_2H_3$], **2a** and **2b**. It is interesting to compare these results with that previously reported for the related Cp* system, which led to a mixture of [MoCp*(PMe_3)$_2H_3$] and [MoCp*(PMe_3)$_3$H].[24] The bulkier Cp$^\#$ systems afford the trihydride derivatives **2** selectively and show no tendency to replace H_2 in the presence of excess PMe_3 under thermolytic conditions.

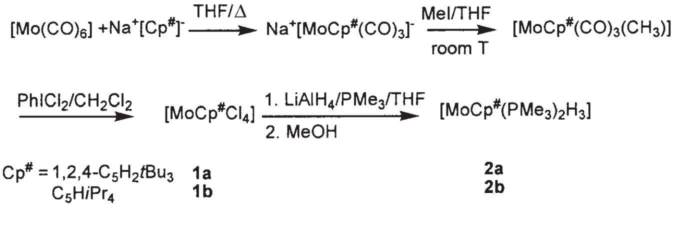

Scheme 1.

Both compounds gave single crystals suitable for a structural analysis. The crystal of **2a** had sufficient quality to allow the location and refinement of the hydride positions from the X-ray data, as shown in the previous communication.[21] We have now completed the structural investigation with a neutron diffraction experiment for **2a** (the results of both refinements are compared in Table 1) and an X-ray diffraction experiment for **2b**. The latter crystals had poorer quality and the hydride positions could not be located; the observable structural parameters are very close to those of **2a**, see Table 1. A view of both geometries is shown in Figure 1. The molecular geometry is unusual for a half-sandwich [Mo(ring)X_3L_2] compound, but parallels that previously reported for the related [MoCp*(dppe)H_3] compound.[25,26] This demonstrates that the unusual structure observed for [MoCp*(dppe)H_3] is not enforced by the chelating nature of the dppe ligand. Another example for this structural type has recently been reported for the isoelectronic compound [WCp*(CO)$_2H_2$(SiH_2Ph)].[27] As expected, the X-ray diffraction experiment yields shorter Mo–H distances than the neutron diffraction experiment for compound **2a**. Only those afforded by neutron diffraction should be considered reliable. The parameters that do not involve hydrogen atom positions, on the other hand, are more precisely determined by the X-ray diffraction experiment.

Table 1. Selected bond lengths [Å] and angles [°] for all structurally characterized complexes.

	2a		**2b**	**3a**	$\mathbf{2a}^+$		**5a**
	X-ray	Neutron	X-ray	X-ray	X-ray[a]	X-ray	
Mo–CNT[b]	2.0150(2)	2.019(5)	2.013(1)	2.0100(2)	1.9992(4)	2.0036(4)	2.0096(3)
Mo–P1	2.3832(6)	2.385(5)	2.377(4)	2.4656(7)	2.4720(14)	2.4744(15)	2.4801(8)
Mo–P2	2.3801(6)	2.377(5)	2.375(4)	2.4720(7)	2.4738(14)	2.4726(15)	2.4685(9)
Mo–H1	1.58(3)	1.712(8)		1.67(3)	1.65(4)	1.60(4)	1.83(3)
Mo–H2	1.57(3)	1.719(9)		1.58(3)	1.52(4)	1.56(4)	
Mo–H3	1.58(3)	1.719(9)		1.61(3)	1.54(4)	1.60(4)	
Mo–H4				1.66(3)			
H2···H3	1.63(4)	1.69(2)			1.33(6)	1.38(6)	
CNT-Mo-P1	130.62(2)	130.7(2)	133.8(1)	120.339(18)	127.80(4)	126.13(4)	122.02(2)
CNT-Mo-P2	132.14(2)	132.1(2)	131.5(1)	120.808(18)	127.16(4)	127.74(4)	121.57(2)
CNT-Mo-H1	106(1)	105.8(3)		108.5(9)	105(2)	104(2)	125.2(9)
CNT-Mo-H2	107(1)	106.0(3)		104.9(9)	107(2)	110(2)	
CNT-Mo-H3	114(1)	115.1(3)		104.7(9)	106(2)	109(2)	
CNT-Mo-H4				173.1(9)			
P1-Mo-P2	93.71(2)	93.6(2)	94.02(14)	112.09(2)	100.25(6)	100.42(6)	109.55(3)
H2-Mo-H3	62(2)	58.9(5)			51(2)	52(2)	

[a] The parameters of each crystallographically independent molecule are shown in separate columns. [b] CNT is the centroid of the Cp ring.

The most interesting structural feature is the distance between atoms H2 and H3 (1.69(2) Å from the neutron structure). This value is too long to envisage an interaction, but short in comparison to most nonbonded distances recorded by neutron diffraction for polyhydride complexes. This is evidence for a certain degree of "compression".[28] Other relatively short nonbonded H···H separations are 1.67(1) and 1.70(1) Å in $[IrCp(PMe_3)H_3]^+$,[29] and values ranging from 1.637(4) to 1.668(4) Å between adjacent H atoms in compound $[Os(P\mathit{i}Pr_2Ph)_2H_6]$,[30] whereas there are no shorter intramolecular H···H separations than 1.77 Å in compound $[Re(dppe)H_7]$.[31] The longest H–H separations in compounds that have been defined as "stretched H_2 complexes" are 1.357(7) Å in $[ReH_7\{P(C_6H_4\text{-}p\text{-}CH_3)_3\}_2]$[32] and 1.34(2) in $[Os(H_2)(en)_2(O_2CMe)]^+PF_6^-$,[33] all these values resulting again from neutron diffraction experiments. Finally, complex $[OsH_5(PMe_2Ph)_3]^+$ exhibits an even longer separation (1.49(4) Å) and was described as falling in a "gray" region in which there may or may not be a direct H/H attractive interaction.[34] The Cambridge Crystallographic Structural Database does not reveal H–H contacts between 1.0 and 1.7 Å for Mo complexes, but a distance of about 1.18 Å has recently been estimated from longitudinal relaxation times (T_1) and J(H,D) measurements for complex $[Mo(NPh)(PMe_3)_2(H_2)(o\text{-}(Me_3SiN)_2C_6H_4)]$.[35] Interestingly, if the H2 and H3 atoms are considered as defining a stretched H_2 ligand, therefore occupying a single coordination position in a Mo^{II} complex, then the coordination geometry would be described as a "four-legged piano stool", which is indeed a quite common geometrical arrangement for Mo^{II},[36] as exemplified by $[MoCp(PMe_2Ph)_3Cl]$[37] and $[MoCp(dppe)(CO)H]$.[38]

The NMR properties of **2a** and **2b** confirm the presence of three hydride ligands. The single $^{31}P\{^1H\}$ resonance observed at room temperature is transformed into a binomial quartet in a ^{31}P\{sel. ^1H\} NMR experiment, showing that the P nuclei are coupled to three equivalent protons. In addition, the ^1H spectrum shows a single, sharp triplet resonance. A rapid exchange process between the inequivalent hydride positions must therefore be present. For the related $[MoCp^*(dppe)H_3]$ compound, the fluxional process could not be frozen out even at the lowest attainable temperatures.[26] For compounds **2a** and **2b**, on the other hand, cooling results in decoalescence for the ^1H NMR signal to yield two signals in a 1:2 ratio, consistent with the solid-state structural investigation, see Figure 2. This shows quite clearly the effect of the bulky ring substituents on the dynamics of the hydride exchange process. For compound **2a**, the lowest temperature (193 K) spectrum displayed well-resolved triplets, due to coupling to the two equivalent P donor nuclei, with the unique hydride ligand being characterized by a greater J(H,P) (64 Hz), relative to the two equivalent ones (44 Hz). No H–H coupling between the inequivalent hydrides can be discerned. For compound **2b**, on the other hand, the spectrum remained rather broad even at 193 K. A line-shape analysis yielded the activation parameters of the hydride scrambling process as $\Delta H^{\ddagger} = 9.0 \pm 0.7$ (**2a**) and $8.5 \pm 0.3\ kcal\,mol^{-1}$ (**2b**); $\Delta S^{\ddagger} = 17 \pm 3$ (**2a**) and 21 ± 1 e.u. (**2b**) e.u. The similar values of both activation parameters for the two compounds are in line with the similar structure of the two compounds. The longitudinal relaxation times (T_1) of the various signals are also shown in Figure 2. They confirm the classical nature of the compounds. Most notably, for compound **2a**, the T_1 value for the equivalent hydride ligands signal is not significantly shorter than that of the unique hydride resonance below the decoalescence temperature.

The ^{31}P NMR resonance of the two phosphane ligands remained sharp in the entire temperature range for compound **2a**, in agreement with the chemical equivalence shown by the X-ray structure. For compound **2b**, on the other hand, a decoalescence phenomenon was observed at low temperatures, yielding two singlet resonances with approximately equal intensities at $\delta = 15.9$ and 12.3 ppm at 193 K (figure

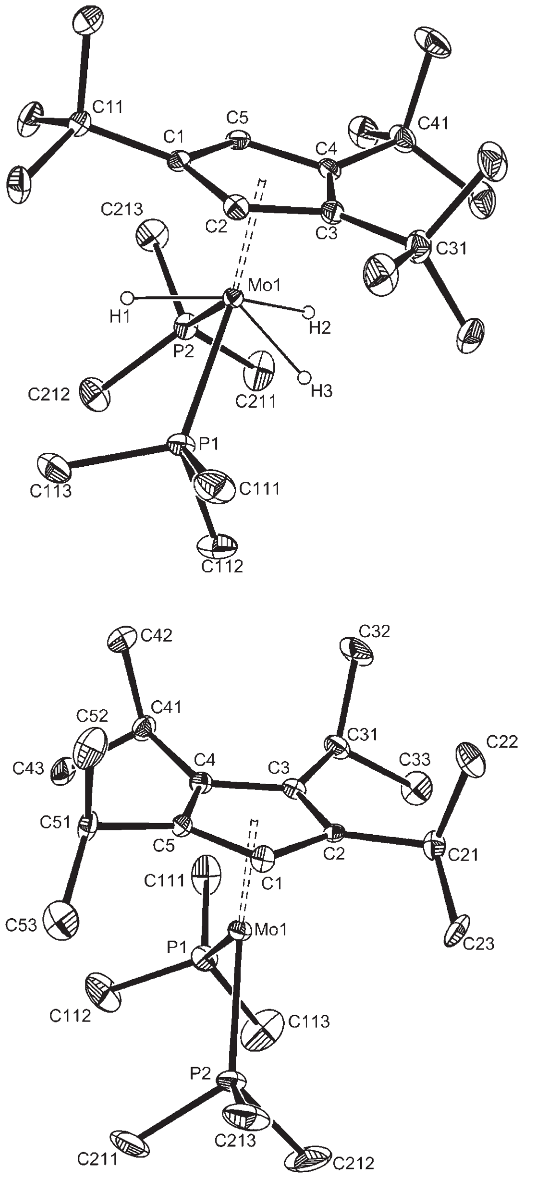

Figure 1. ORTEP view of compounds **2a** (neutron diffraction, top) and **2b** (bottom). Hydrogen atoms, except those directly bonded to the Mo atom in compound **2a**, are not shown for clarity.

shown in the Supporting Information). This behavior can be rationalized by either the freezing out of a single Mo-(C_5HiPr_4) rotamer with symmetry inequivalent PMe_3 donors (but these ligands also need to be characterized by a small enough P–P coupling, since this is not observed at 193 K), or by the presence of two equilibrating rotamers having similar energy, perhaps differing by the relative conformation of the *i*Pr groups in the C_5HiPr_4 ring. The latter phenomenon would not be expected to lead to the existence of different rotamers for the 1,2,4-$C_5H_2tBu_3$-substituted complex.

Protonation studies: Compound **2a** reacts with HBF_4 at −80 °C in THF to yield the tetrahydride complex $[Mo(1,2,4\text{-}C_5H_2tBu_3)H_4(PMe_3)_2]^+BF_4^-$ (**3a**), see Scheme 2. This product is related to the previously described $[MoCp^*(dppe)H_4]^+$,[26] but shows a much greater thermal stability. It is stable in THF at room temperature, whereas complex $[MoCp^*(dppe)H_4]^+$ decomposes rapidly by loss of H_2 via a presumed nonclassical $[MoCp^*(dppe)(H_2)H_2]^+$ intermediate. This stabilization effect is probably related to the greater donor power of the coordination sphere in **3a** relative to $[MoCp^*(dppe)H_4]^+$, with the corresponding stabilization of the classical tetrahydrido structure with respect to the nonclassical tautomer. Compound **3a** is diamagnetic and colorless, as expected for the d^0 configuration of formally hexavalent molybdenum. It features, as expected, a triplet hydride signal in the ^1H NMR spectrum (at −4.2 ppm) and a singlet (at 0.6 ppm) in the $^{31}P\{^1H\}$ NMR spectrum. Selective irradiation of the PMe_3 proton resonance yields a quintet ^{31}P signal, in agreement with the presence of four hydride ligands. The compound has also been structurally characterized by single-crystal X-ray diffraction.

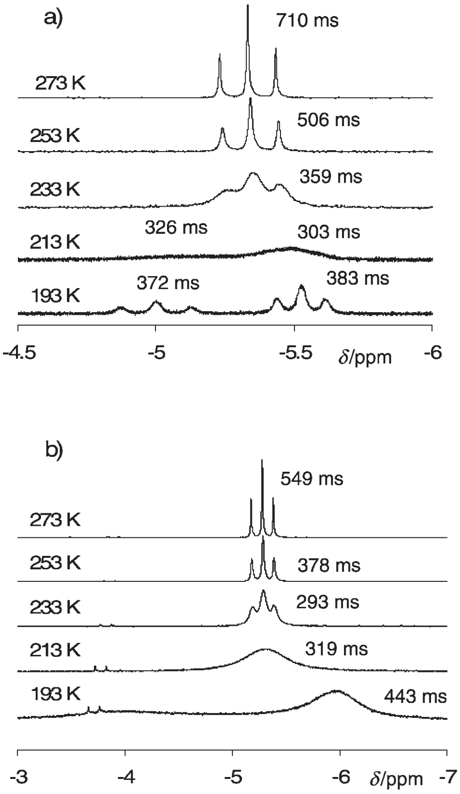

Figure 2. Variable-temperature ^1H NMR spectrum of a) compound **2a** and b) compound **2b** in the hydride resonance region. The individual temperatures are shown on each spectrum and the time values shown are the longitudinal relaxation times of the corresponding resonance.

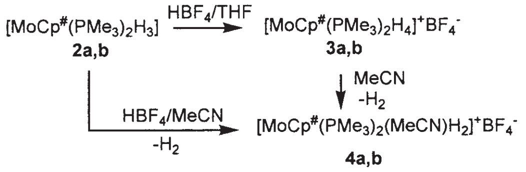

Scheme 2.

The cation geometry is illustrated in Figure 3. The crystal quality allowed the location and refinement of all four hydride ligands. The geometry of the tetrahydride cation can be described as a highly distorted pentagonal bipyramid if the bulky 1,2,4-$C_5H_2t\text{Bu}_3$ ligand is considered to occupy a single coordination position at one of the vertices of the bipyramid. The second axial position is occupied by the hydride ligand H4, with the five equatorial ligands bent toward H4 and away from the cyclopentadienyl ligand (especially the two phosphine ligands, for steric reasons). The two PMe_3 ligands occupy 1,3-positions in the pseudo-pentagonal plane, with atom H1 bisecting the P1-Mo-P2 angle. The related complex $[WCp^*(dppe)H_4]^+$ was found to adopt an analogous coordination geometry, with the chelating dppe ligand occupying one equatorial and one axial site.[26]

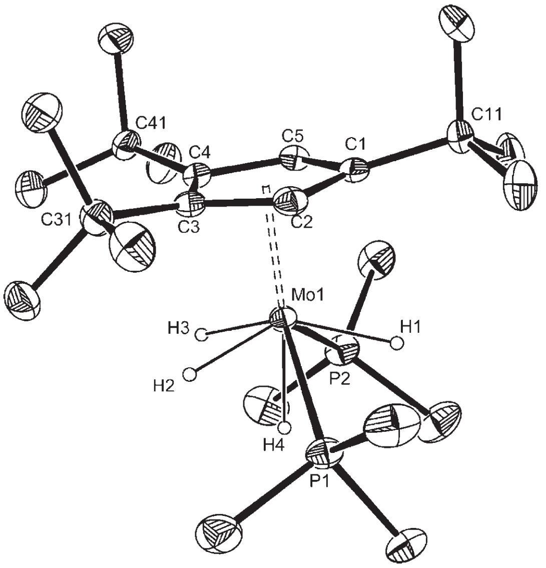

Figure 3. ORTEP view of the cation in compound **3a**. Hydrogen atoms, except those directly bonded to the Mo atom, are not shown for clarity.

The cationic tetrahydride complex **3a** was also formed by protonation of **2a** with HBF_4 in MeCN, but further rapid evolution took place in this case. This reaction was only carried out on a spectroscopic scale in CD_3CN and the resulting solution was monitored with time by ^1H and ^{31}P NMR spectroscopy. Within minutes at room temperature, resonances corresponding to a second complex began to appear and the conversion was complete in 5 h. This product, $[Mo(1,2,4\text{-}C_5H_2t\text{Bu}_3)(PMe_3)_2(MeCN)H_2]^+$ (**4a**) derives from H_2 elimination/MeCN coordination from **3a**. It displays a singlet $^{31}P\{^1H\}$ resonance at 1.85 ppm, which converts into a triplet upon selective decoupling of the PMe_3 ligand ^1H resonance. At room temperature a single broad hydride resonance is observed; however, on cooling a solution of **4a** in CD_3CN to −40° C, two triplet hydride resonances are resolved at −0.27 and −6.77 ppm respectively. This suggests that the two PMe_3 ligands occupy equivalent positions at all temperatures, consistent with the structure **I**.

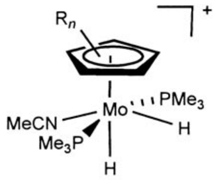

I R_n = 1,2,4-*t*Bu$_3$, *i*Pr$_4$

The corresponding reaction of **2b**, when carried out in THF at −80 °C, led to the precipitation of a white solid, presumably corresponding to the $[Mo(C_5Hi\text{Pr}_4)(PMe_3)_2H_4]^+$ complex, **3b**. However, this compound decomposes, even in the solid state, when warmed up to room temperature. Therefore, it could not be spectroscopically characterized. When the same protonation reaction was carried out in acetonitrile, the formation of complex $[Mo(C_5Hi\text{Pr}_4)(PMe_3)_2(MeCN)H_2]^+$ (**4b**) could be observed. As with **4a**, the hydride ligands in complex **4b** are involved in a fluxional process at room temperature, appearing as a very broad resonance at −2.5 ppm. On cooling to 200 K in [D$_6$]acetone, two doublet of triplet resonances decoalesce, at −0.13 and −5.27 ppm, confirming that each hydride ligand couples to two equivalent phosphorus nuclei and to the other hydride ligand, in agreement with structure **I**. At this temperature, all four isopropyl groups on the cyclopentadienyl moiety also become inequivalent. In both complexes **4a**,**b**, a resonance integrating to three protons, assigned to the coordinated MeCN, can be observed at $\delta = 2.17$ (for **4a** in CD_3CN) and 2.71 ppm (for **4b** in [D$_6$]acetone). This behavior is analogous to that of the related $[MoCp^*(dppe)H_3]$ complex.[26] The greater coordinating ability of the acetonitrile solvent induces a more facile H_2 elimination by more efficiently trapping the resulting 16-electron fragment.

Oxidation studies—isolation and characterization: Preliminary electrochemical investigations indicated that both complexes **2a**,**b** undergo an electrochemically reversible one-electron oxidation process and suggested that the oxidation product is relatively stable. The electrochemical behavior will be analyzed in more detail in a later section. The stoichiometric oxidation was accomplished by the use of $[FeCp_2]^+[PF_6]^-$ in THF, see Scheme 3. The product for the 1,2,4-$C_5H_2t\text{Bu}_3$ system was sufficiently stable to be isolated and crystallized. Its X-ray structure and its EPR spectrum (Figure 4) demonstrate its chemical identity as the PF_6^- salt of the one-electron oxidation product **2a**$^+$, as discussed previously.[21]

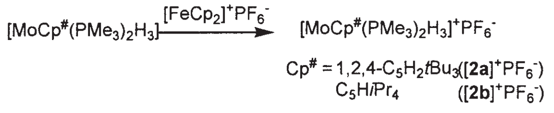

Scheme 3.

The most relevant metric parameters of the **2a**$^+$ structure are compared with those of the parent compound **2a** in Table 1. The overall geometry of the cation is essentially unchanged relative to that of the neutral precursor (see the previous communication for an ORTEP view).[21] There is

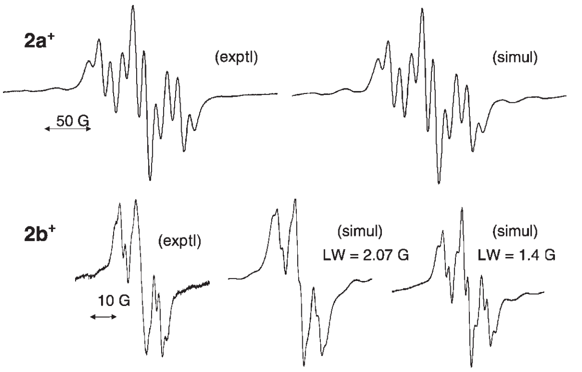

Figure 4. EPR spectra of complexes 2^+ in THF. Above: complex $\mathbf{2a}^+$ ($T=193$). Below: complex $\mathbf{2b}^+$ ($T=183$).

no evidence of an interaction between the two ions, notably hydrogen bonding between the hydride ligands and the fluorine atoms of the anion. The Mo–CNT distance is slightly shorter, whereas the Mo–P distances are slightly longer, relative to the neutral precursor. The most notable change is a decrease of the H2···H3 contact from 1.69(2) Å (neutron diffraction) or 1.63(4) Å (X-ray diffraction) in the neutral complex to an average of 1.36(6) Å (from the X-ray data) in the cation. The difference is significant at the 2σ level relative to the X-ray structure, at the 4σ level relative to the neutron structure. Unfortunately, suitable crystals of compound $\mathbf{2a}^+PF_6^-$ for a neutron diffraction analysis could not be grown. Even when keeping the uncertainty into account, however, the H2···H3 separation in the cationic complex falls inside the range of compounds that have previously been described as “stretched” or “elongated” dihydrogen complexes, or alternatively as “compressed” dihydrides.[28,39] Thus, it appears that the oxidation process has increased the interaction between the two hydride ligands H2 and H3.

Compound $\mathbf{2a}^+PF_6^-$ appears to be the first reported paramagnetic polyhydride complex showing evidence for a stretched dihydrogen ligand (or compressed MH_2 system). It is interesting to compare this structure with that of the previously published isoelectronic $[WCp^*(dppe)H_3]^+$ complex.[9] The two systems show a very different arrangement of the three hydride ligands, the closest H···H contact in the tungsten complex being 2.11 Å. Although the H positions in this tungsten complex should again be considered with caution, since this structure was also obtained from X-ray diffraction data, the relative arrangement of the heavy atoms that define the coordination sphere (the Cp ring, the metal, and the P donor atoms) is quite different in the two compounds. As we know, the W complex is stable and has no tendency to decompose, notably by H_2 elimination.

The oxidation product obtained from **2b** is rather short-lived at room temperature and could not be isolated. It was only characterized in situ by EPR spectroscopy, see Figure 4. Like $\mathbf{2a}^+$, it exhibits a rather broad spectrum at ambient temperature, which becomes sufficiently resolved at lower temperatures to allow the identification of the expected quartet of triplet feature, consistent with the presence of two phosphorus donor atoms and three hydride ligands, flanked by the ^{95}Mo and ^{98}Mo isotope satellites. This suggests, like for the 1,2,4-tBu$_3$ analogue, that one-electron oxidation has afforded complex $\mathbf{2b}^+$.

The spectroscopic properties, however, are peculiar in many respects. The simulation on the basis of any combination of spin ½ nuclei different than P_2H_3 (for instance, 2P and 2H) failed to provide a spectrum sufficiently resembling the experimental one. However, the simulation for the P_2H_3 spin system was not nearly as satisfactory as for the $\mathbf{2a}^+$ homologue. An unrestricted full parameter optimization resulted in too broad lateral features and a too sharp central one, compared to the experimental spectrum (Figure 4), for a linewidth (LW) of 2.07 G. An artificial reduction of the line broadening parameter to 1.4 G allows a perfect match of the two lateral features of the triplet, but the central feature becomes too sharp relative to the experiment. This may indicate a dynamic exchange process on the EPR timescale. Indeed, virtual triplets displaying artificially broadened central features are commonly found in the NMR spectra of diamagnetic compounds featuring suitable site exchange phenomena, such as the X signal for an ABX system, in which sites A and B are near the fast exchange limit.[40,41] A rapid hydride scrambling process takes place for $\mathbf{2a}^+$ (symmetric EPR coupling pattern, inequivalent hydride positions by X-ray crystallography), as well as for the neutral precursors (vide supra) and for the related $[MoCp^*(dppe)H_3]^{n+}$ ($n=0$, 1) complexes.[9] This exchange is possibly slower for the more encumbered $C_5H\mathit{i}Pr_4$ derivative, causing the observed lineshape effect. It is interesting to note that the exchange rates are similar for the neutral precursors (slightly smaller for **2a**), whereas the exchange process appears faster in $\mathbf{2a}^+$ than in $\mathbf{2b}^+$.

The next peculiar feature of the EPR spectrum of $\mathbf{2b}^+$ is a much lower value found for the a_P and a_H parameters (namely $a_P=6.2$ G; $a_H=1.7$ G; $a_{Mo}=29.4$ G) relative to both $\mathbf{2a}^+$ ($a_P=36.2$ G, $a_H=11.4$ G, $a_{Mo}=30.8$ G)[21] and $[MoCp^*(dppe)H_3]^+$ ($a_P=29.8$ G; $a_H=11.8$ G).[9] The cause of this phenomenon is not quite clear, but the different coupling values suggest that $\mathbf{2b}^+$ adopts a different geometry with respect to that of $\mathbf{2a}^+$, possibly involving the complete collapse of two hydrides to a dihydrogen ligand. It is easy to imagine how the greater bulk of the substituted cyclopentadienyl ring in $\mathbf{2b}^+$ might force the two hydrogen atoms closer together. This phenomenon may well be related to the slower hydride mutual exchange, as well as to our inability to isolate the compound. Related to this point, we recall that the tetrahydride protonation product is stable in the case of **3a** but decomposes in the case of **3b**, although the same system **4a**,**b** is obtained in MeCN. Thus, we speculate that the extreme bulk of the $C_5H\mathit{i}Pr_4$ ligand has the effect of pushing out an H_2 ligand from both systems **3b** and $\mathbf{2b}^+$.

Oxidatively induced H_2 reductive elimination: Although compound $\mathbf{2a}^+PF_6^-$ is quite stable as a crystallized solid and in THF at low temperatures, it slowly decomposed at $T>0$ °C, as indicated by a color change from orange to green. Well formed green crystals were obtained by slow crystallization from THF/pentane at −20 °C. This product appeared thermally stable with no noticeable change over time in the solid state and in THF at room temperature. X-ray diffraction analysis revealed the identity of the compound as $[Mo(1,2,4\text{-}C_5H_2\mathit{t}Bu_3)\text{-}(PMe_3)_2H]^+PF_6^-$ (**5a**). A view of the structure is presented in our previous communication,[21] while selected bonding parameters are reported in Table 1. Therefore, the compound derives from its precursor $\mathbf{2a}^+PF_6^-$ by H_2 elimination, see Scheme 4.

$$[Mo(1,2,4\text{-}C_5H_2\mathit{t}Bu_3)(PMe_3)_2H_3]^+PF_6^- \xrightarrow[-H_2]{\text{THF, 0°C}} [Mo(1,2,4\text{-}C_5H_2\mathit{t}Bu_3)(PMe_3)_2H]^+PF_6^-$$

Scheme 4.

Although the quality of the data set allowed the identification of a single hydride ligand with a high level of confidence (see Experimental Section), the question of the possible presence of additional hydride ligands in the structure of compound **5a** has been considered carefully, since hydrogen atoms may be difficult to locate from X-ray diffraction data. Possibilities include the presence of one, two, or three additional hydride ligands, giving a 16-electron dihydride, a 17-electron trihydride (a stereoisomer of the precursor $\mathbf{2a}^+$), and an 18-electron tetrahydride cation (i.e. complex **3a**), as well as a dihydrogen ligand, yielding a nonclassical tautomer of $\mathbf{2a}^+$. The color of **5a** relative to $\mathbf{2a}^+PF_6^-$ excludes an isomeric form of $\mathbf{2a}^+$ and also the tetrahydride formulation, although the bond lengths and angles related to the heavy atoms in the cation of **5a**, see Table 1, are not too different from those observed for compound **3a**.

The ^1H NMR spectrum of the isolated solid only revealed the resonances of the tetrahydride complex **3a**, indicating that this compound is a decomposition byproduct (the solid was a mixture of well-formed crystals and a powder). Complex **3a** certainly arises from the transfer of a proton from acidic $\mathbf{2a}^+$ to residual **2a**, similarly to what occurs for the $[MoCp^*(dppe)H_3]$ analogue.[16] A solid sample of the isolated compound showed bulk paramagnetism; however, a reliable value for the magnetic moment could not be obtained, given the impure nature of the sample. ^1H NMR monitoring of the decomposition reaction also showed the formation of **3a**, in addition to the formation of H_2.

Positive identification of the green decomposition product as a 15-electron species comes from EPR spectroscopy. As detailed in the communication,[21] the solid sample shows features consistent with a spin quartet ground state at the liquid He temperature (Figure 5a): g_x and g_y at 3.74 and 3.45 ($\pm\frac{1}{2}$ transition), plus a weak feature (g_z for the forbidden $\pm\frac{3}{2}$ transition) at 5.33. The $g=3.74$ peak appears to display a fine structure, possibly due to coupling to the two equivalent P nuclei. The g_z component of the $\pm\frac{1}{2}$ transition is not visible because it is overshadowed by stronger resonances in the $g=2$ region (shown in Figure 5b). The resonance observed at $g=2.009$ for the polycrystalline sample is very close to the position observed at higher temperature for the precursor complex $\mathbf{2a}^+$ and is therefore attributed to a residual amount of this material, which had co-crystallized with the H_2 elimination product **5a** (see Experimental Section).

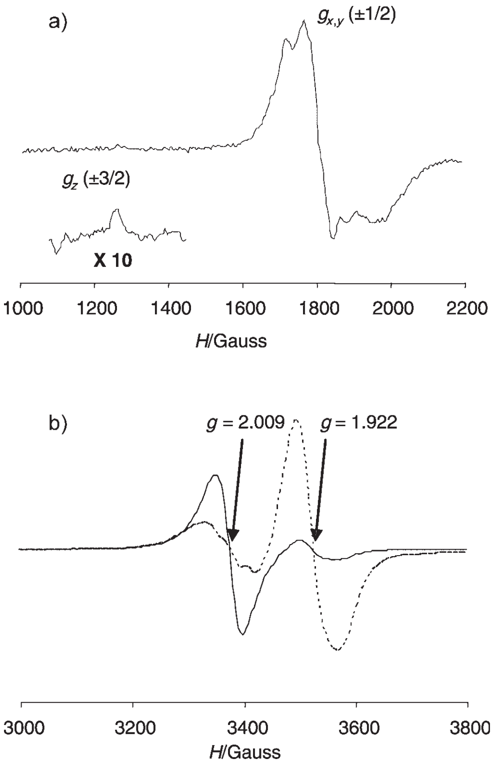

Figure 5. Liquid He EPR spectrum of compound **5a**: a) polycrystalline sample in the $g=4$–6 region; b) polycrystalline sample (solid line) and frozen THF glass (dashed line) in the $g=2$ region.

Solutions of compound **5a** in THF were EPR silent at room temperature and showed only a weak resonance at the liquid-nitrogen temperature. On the other hand, they show an intense band at $g=1.922$ at the liquid-helium temperature. The two resonances at $g=2.009$ and 1.922 are visible for both polycrystalline and solution samples in THF, but their relative intensity is opposite. The latter must belong to another $S=\frac{1}{2}$ complex and we therefore assign it to the THF adduct, $[Mo(1,2,4\text{-}C_5H_2\mathit{t}Bu_3)(PMe_3)_2(thf)H]^+$. Its presence for the polycrystalline sample, which had been obtained by crystallization from THF (see Experimental Section), represents evidence of solution equilibrium between the solvent-free, 15-electron, spin-quartet monohydride complex and a spin-doublet solvent adduct. The compound crystallizes preferentially in the solvent-free form, but the THF adduct also appears to exist in the solid state. Additional evidence for this equilibrium will be provided by the electrochemical analysis (vide infra).

As stated in the Introduction, we previously reported the first unambiguous oxidatively induced reductive elimination of H_2 from the one-electron oxidation of complex $[MoCp^*(dppe)H_3]$.[9] However, the elimination product could not be crystallized and was only characterized in solution as the 17-

electron solvent adduct $[MoCp^{*}(dppe)(solv)H]^{+}$ by EPR spectroscopy (solv = THF, CH_2Cl_2)[9] and by electrochemistry (solv = MeCN).[16] The steric bulk of the PMe_3 and 1,2,4-$C_5H_2tBu_3$ ligands, in combination with the electron-pairing stabilization provided by the spin-quartet state,[42,43] accounts for the absence of solvent coordination to complex **5a**. The oxidatively induced reductive elimination of compounds containing two one-electron ligands ([M(X)(Y)], leading to the elimination of X−Y) has previously been demonstrated for dialkyl complexes $[M(R)_2]$ to give the alkane coupling product R−R[18,44–50] and for alkyl-hydride complexes [M(R)(H)] to give the corresponding alkane R−H,[18,47] plus products originating from $[M]^{+}$. To the best of our knowledge, the 15-electron $[M]^{+}$ product was not isolated and characterized in any of those studies. For X = Y = H, as stated in the Introduction, oxidation often results in dihydrogen evolution, but the multitude of decomposition pathways of the intermediate oxidized polyhydride complexes often obscure the clean identification of the oxidatively induced reductive elimination pathway. Therefore, the present investigation illustrates the first well-defined example of an oxidatively induced reductive elimination of H_2, through the full characterization of starting and end product of the H_2 elimination process.

Since the greater bulk of the C_5HiPr_4 ring should cause an even more favorable H_2 elimination process, the decomposition of the less thermally stable $\mathbf{2b}^{+}$ would be expected to lead to another 15-electron monohydride species, **5b**, analogous to **5a**. Upon warming to room temperature, orange solutions of $\mathbf{2b}^{+}$ change color to blue, but the transformation is accompanied by the development of new EPR signals indicative of other $S = \frac{1}{2}$ species, which replaced the signal of the cationic trihydride complex. Thus, this decomposition is less well behaved than that of $\mathbf{2a}^{+}$, which led to an EPR silent solution (at room temperature). We cannot exclude the presence of species **5b** in this solution, but attempts to crystallize one or more of the decomposition products from this solution were unsuccessful.

Electrochemical studies: Compounds **2a**,**b** exhibit a reversible one-electron oxidation in both THF and MeCN at the usual scan rates. The measured $E_{1/2}$ values for **2a** and **2b** are very similar (**2a**: −0.93 V in MeCN, −0.89 V in THF; **2b**: −0.95 V in MeCN, −0.88 in THF vs. the ferrocene standard). These potentials are slightly more negative than those measured for the related $[MoCp^{*}(dppe)H_3]$ compound (−0.85 V in MeCN and −0.73 V in THF)[9] in agreement with the greater electron-donating power of the coordination sphere. While the process is reversible in THF for scan rates as low as $10\,mV\,s^{-1}$ for both compounds, the back reduction wave loses intensity relative to the oxidation wave at slow scan rates in MeCN. A figure is provided in the Supporting Information.

The cyclic voltammetry of compounds **2a** and **2b** has been investigated in MeCN and THF at variable scan rates and different potential ranges. The observed behavior is closely related to that of complex $[MoCp^{*}(dppe)H_3]$,[9,16] a detailed study of which revealed three simultaneous decomposition pathways for the one-electron oxidation product, $[MoCp^{*}(dppe)H_3]^{+}$: deprotonation, disproportionation, and H_2 elimination. Each pathway could be independently quantified (e.g. $k_{deprot} = 2.8(2)\times10^{2}\,s^{-1}\,M^{-1}$, $k_{disp} = 3.98(9)\times10^{3}\,s^{-1}\,M^{-1}$ and $k_{elim} = 2.0(4)\times10^{-2}\,s^{-1}\,M^{-1}$ in MeCN).[9,16] For complexes **2a** and **2b**, we did not carry out a thorough quantitative study. Rather, we focused only the voltammetric features that could provide additional information about the H_2 elimination pathway.

All three decomposition pathways of $[MoCp^{*}(dppe)H_3]^{+}$ have an associative character: disproportionation is initiated by solvent coordination to the 17-electron $[MoCp^{*}(dppe)H(H_2)]^{+}$ isomer; deprotonation needs the involvement of a molecule of neutral, 18-electron $[MoCp^{*}(dppe)H_3]$; and H_2 elimination follows initial MeCN coordination.[16] Indeed, the H_2 elimination is much slower in THF ($k_{elim} = 2.2(2)\times10^{-5}\,s^{-1}\,M^{-1}$; measured independently by decay of the EPR signal),[9] with no visible consequence on the cyclic voltammetric behavior in this solvent. Since compounds **2a** and **2b** have a more crowded coordination sphere than $[MoCp^{*}(dppe)H_3]$, the above three pathways should be slower. However, whereas both disproportionation and deprotonation pathways demand a rate-determining associative step, the H_2 elimination may also occur dissociatively, in which case the greater ligand steric pressure should accelerate it. We remind here that compound **5a** is the stable product of H_2 dissociation from $\mathbf{2a}^{+}$, although equilibrium amounts of the solvent adduct are present in THF (see EPR characterization above). This suggests a dissociative H_2 elimination process in THF, but does not exclude an associative process in MeCN.

A two-scan cyclic voltammogram of **2a** at a scan rate of $5\,V\,s^{-1}$ is shown in Figure 6. When the scan is reversed at 0.7 V (vs. the reference Ag/AgCl electron, that is, 0.27 V vs. ferrocene), only an additional oxidation peak **B** at −0.10 V (−0.05 V for **2b**) is observed in the voltammogram, in addition to the reversible one-electron oxidation of **2a** at **A**/**A′**. There is no return wave associated to this peak, indicating that the generated species decomposes rapidly. Note that the voltammogram does not change significantly in the second scan. When the potential sweep is switched at a

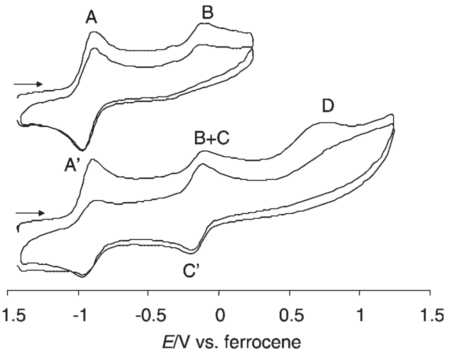

Figure 6. Two-scan cyclic voltammograms of compound **2a** in MeCN. Scan rate = $5000\,mV\,s^{-1}$.

higher potential, on the other hand, a third oxidation process **D**, also irreversible, appears at approximately 0.8 V. Following the first potential sweep reversal, a new reversible process at **C**/**C′** becomes visible at $E_{1/2} = -0.15$ V (-0.10 V for **2b**). Oxidation peak **C** overlaps with peak **B** in the second scan. The behavior of compound **2b** is very similar to that of **2a**. The **C**/**C′** process shows a reduced reversibility for compound **2b**. Voltammograms of **2a** and **2b** at variable scan rates are available in the Supporting Information.

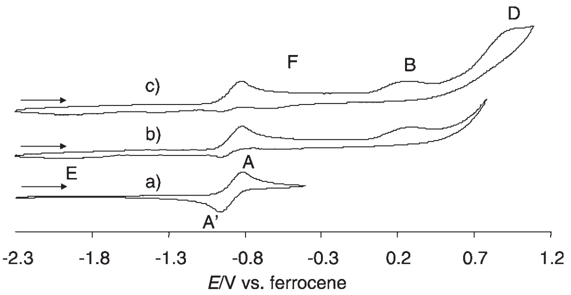

Figure 7. Cyclic voltammograms of compound **2a** in THF with different switching potentials. Scan rate = 200 mV s^{-1}.

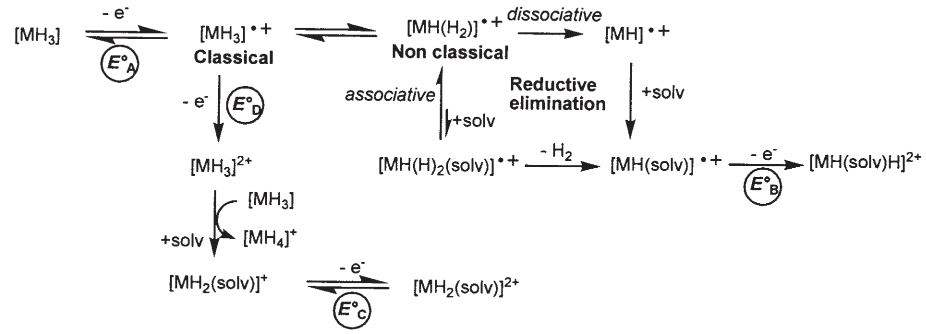

Scheme 5.

According to the previous study, the above observations are interpreted as follows, see Scheme 5. The 17-electron $[MH_3]^{+\cdot}$ complex produced at **A** yields (via the nonclassical isomer $[MH(H_2)]^{\cdot+}$) complex $[MH(MeCN)]^{\cdot+}$, which is responsible for the oxidation peak **B**. The complete lack of reversibility for the latter is due to the immediate saturation by solvent coordination, to afford the 18-electron $[MH(MeCN)_2]^{2+}$. On the other hand, subsequent oxidation of $[MH_3]^{\cdot+}$ at **D** leads to the 16-electron $[MH_3]^{2+}$, which is immediately followed by proton transfer to the starting material $[MH_3]$ with formation of $[MH_4]^+$ (redox inactive) and $[MH_2(MeCN)]^+$. The latter is responsible for the reversible process **C**/**C′**. A deeper analysis of these processes and complimentary investigations confirming their assignment were carried out during the previous study.[16] The two anodic waves of peaks **B** and **C** accidentally overlap for M = Mo(1,2,4-$C_5H_2tBu_3$)(PMe_3)$_2$, whereas they differ only slightly for M = MoCp*(dppe) ($\Delta E = 0.14$ V).[16] The essentially identical potentials measured for 17-electron $[MH(MeCN)]^{\cdot+}$ and 18-electron $[MH_2(MeCN)]^+$ agree with a high covalent nature for the Mo–H bond.

The essential point is that peak **B** is observed even at the highest scan speeds (up to 5 V s^{-1}), whereas the same process for system [MoCp*(dppe)H_3] became observable only at $v < 0.6$ V s^{-1} in neat MeCN. This illustrates that the H_2 elimination process is fast for systems $\mathbf{2a}^+$ and $\mathbf{2b}^+$, faster than when M = MoCp*(dppe), thus strongly suggesting that it proceeds dissociatively.

The voltammograms of **2a** in THF, see Figure 7, show many similarities, but also interesting differences with respect to the behavior of the same compound in MeCN and to that of compound [MoCp*(dppe)H_3] in THF. Following the oxidation at **A**, the irreversible peak **B** and the second oxidation process **D** are observed like in MeCN. Transit over process **D** does not generate a reversible **C**/**C′** couple. Transit over process **B**, on the other hand, generates a weak and broad reduction peak **E** at about -1.9 V, while peak **A** loses reversibility. A full rationalization of all these observations is not possible, as many of the species implicated in Scheme 5 may be unstable and evolve to other unknown products when solv = THF. Whereas the potentials of peaks **A** and **D** are close to the values observed in MeCN, peak **B** occurs at $E_{p,a}$ about 0.25 V in THF (vs. -0.18 V in MeCN). The more positive potential in THF may be related to a reduced donating power of THF relative to MeCN and/or to a more extensive solvent dissociation equilibrium established by the THF adduct with the 15-electron complex. Indeed, the presence of this equilibrium has been evidenced by the EPR study (see above). The most interesting feature, however, is the fact that compound **2a** shows peak **B** also in THF, whereas compound [MoCp*(dppe)H_3] only shows it in MeCN.[16] This is consistent with a dissociative mechanism for the H_2 substitution in $\mathbf{2a}^+$, in which case the rate should be essentially solvent independent. Indeed, peak **B** is observable in THF even at the fast scan rates (1 V s^{-1}).

The behavior of **2b** in THF shows similarities to that of **2a** (see figure in the Supporting Information). Notably, a peak corresponding to process **B** is again present ($E_{p,a} = 0.2$ V vs. ferrocene). The behavior at higher potential, however, is more complex and not fully understood. It is possible that only a fraction of $\mathbf{2b}^+$ undergoes H_2 elimination, in competition with other decomposition processes, in the THF solvent. This seems to be suggested also by the EPR monitoring of this decomposition (vide supra). It seems clear, however, that the first decomposition mode (H_2 elimination to afford a 15-electron derivative, possibly in equilibrium with a 17-electron THF adduct) is also established by this system.

Conclusion

We have shown that the combination of greater ligand donor power and greater steric bulk in the coordination sphere of half-sandwich Mo^{IV} trihydride complexes stabilizes the 17-electron products of one-electron oxidation. Complex $[Mo(1,2,4\text{-}C_5H_2\mathit{t}Bu_3)(PMe_3)_2H_3]^+$ is sufficiently stable to be crystallized and structurally characterized. Its geometry is very close to that of the neutral precursor, except that the separation between two hydride ligands is shorter suggesting the presence of a stretched dihydrogen ligand (or compressed MH_2 moiety). To the best of our knowledge, this is the first time that such evidence has been obtained for a paramagnetic polyhydride system. The steric control in this system, however, is rather subtle: on going from the 1,2,4-$C_5H_2\mathit{t}Bu$ system to the more encumbered $C_5H\mathit{i}Pr_4$ system, the paramagnetic trihydride product becomes less stable and could not be isolated. The $C_5H\mathit{i}Pr_4$ ligand might impose such steric pressure to the MoH_3 system as to force a stronger interaction between two hydride ligands and a more favorable expulsion of H_2. This also appears true for the tetrahydrido protonation product (**3a** vs. **3b**). A peculiar difference between the ground-state properties of **2a**$^+$ and **2b**$^+$ has been evidenced by EPR spectroscopy (Figure 4). The present investigation has also revealed a dissociative pathway for H_2 substitution by a solvent molecule in the paramagnetic system. The oxidative behavior of the half-sandwich Mo trihydride system is summarized in Scheme 6: H_2 substitution by MeCN on $[MH_3]^+$ is associative for M = MoCp*(dppe) and dissociative for M = $MoCp^{\#}(PMe_3)_2$; an equilibrium has been established by EPR spectroscopy for the latter system between the 15-electron species (complex **5a**) and its solvent adduct in THF, whereas no evidence was previously obtained for a 15-electron species in the MoCp*(dppe) case. The dissociative product has in fact been isolated and structurally characterized, providing the first well-characterized example of an oxidatively induced reductive elimination of H_2 from a polyhydride compound.

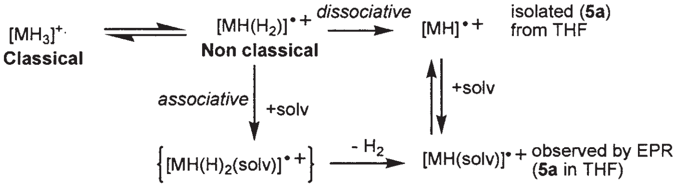

Scheme 6.

Experimental Section

General procedures: All operations were carried out under an atmosphere of argon using standard Schlenk line and glove box techniques. Solvents were dehydrated (CH_2Cl_2: CaH_2; THF, toluene: sodium benzophenone ketyl) and distilled under dinitrogen prior to use. $[Mo(CO)_6]$ and PMe_3 (1 M solution in THF) were purchased from Aldrich and used as received. Compounds 1,2,4-tri(*tert*-butyl)- and tetra(*iso*-propyl)-cyclopentadiene (as isomer mixtures) were prepared by literature methods[51,52] and converted to their corresponding sodium salts by reaction with $NaNH_2$.

Measurements: NMR measurements were carried out on either a Bruker AC 200 or a Bruker AMX250 spectrometer and calibrated with the residual solvent resonances (^1H) or with external 85 % H_3PO_4 (^{31}P). The line-shape analyses for the dynamic processes were carried out by simulation with DNMR3, which is incorporated into the freely available SpinWorks program.[53] EPR spectra were measured on a Elexsys E500 BRUKER spectrometer equipped with both a frequencymeter and gaussmeter. The spectrometer frequency was calibrated with diphenylpicrylhydrazyl (DPPH, $g=2.0037$). EPR spectra simulations and fittings were carried out with the freely available WinSim program.[54] Cyclic voltammograms were recorded with an EG&G 362 potentiostat connected to a Macintosh computer through MacLab hardware/software. The electrochemical cell was fitted with an Ag/AgCl reference electrode, a platinum disk working electrode and a platinum wire counter-electrode. $[Bu_4N]PF_6$ (ca. 0.1 M) was used as supporting electrolyte. The ferrocene standard had a potential of 0.43 V in MeCN and 0.62 V in THF under our experimental conditions.

Synthesis of $[Mo(1,2,4\text{-}C_5H_2\mathit{t}Bu_3)(CO)_3CH_3]$: A solution of $Na(1,2,4\text{-}C_5H_2\mathit{t}Bu_3)$ (1.95 g, 8.3 mmol) in THF (20 mL) was transferred into a suspension of $[Mo(CO)_6]$ (2.20 g, 8.3 mmol) in THF (15 mL). The mixture was heated to reflux for 15 h, during which time a color change from pale yellow to dark red was observed. The mixture was then cooled and CH_3I (1 mL,16 mmol) was added by syringe, causing an immediate color change to bright yellow. Subsequently, the mixture was heated to reflux for 2 h, following which it was cooled and the solvents evaporated. The residue was then extracted with pentane (100 mL) and the pentane solution evaporated to yield $[Mo(1,2,4\text{-}C_5H_2\mathit{t}Bu_3)(CO)_3CH_3]$ as a yellow solid. Yield: 2.642 g; (74 %); IR (CH_2Cl_2): $\tilde{\nu}=2005$, 1918 cm^{-1} (CO).

Synthesis of $[Mo(C_5H\mathit{i}Pr_4)(CO)_3CH_3]$: A solution of $Na(C_5H\mathit{i}Pr_4)$ (2.82 g, 11.0 mmol) in THF (25 mL) was transferred into a suspension of $[Mo(CO)_6]$ (2.88 g, 10.9 mmol) in THF (20 mL). The mixture was heated to reflux for 16 h, during which time a color change from pale yellow to dark red was observed. The mixture was then cooled and CH_3I (1.5 mL, 24 mmol) was added by syringe, causing an immediate color change to bright yellow. Subsequently, the mixture was heated to reflux for 2 h; following which it was cooled and the solvents evaporated. The residue was then extracted with pentane and the pentane solution evaporated to yield $[Mo(1,2,4\text{-}C_5H_2\mathit{t}Bu_3)(CO)_3CH_3]$ as a yellow solid. Yield: 3.739 g (80 %). The compound was used directly for the synthesis of $[Mo(C_5H\mathit{i}Pr_4)Cl_4]$ (see below), without characterization.

Synthesis of $[Mo(1,2,4\text{-}C_5H_2\mathit{t}Bu_3)Cl_4]$ (1a): A solution of $PhICl_2$ (5 g, 38.2 mmol) in dichloromethane (20 mL) was transferred slowly into a solution of $Mo(1,2,4\text{-}C_5H_2\mathit{t}Bu_3)(CO)_3CH_3$ (2.64 g, 6.2 mmol) in dichloromethane (15 mL). The mixture was heated to reflux for 3 h during which time a color change from brown to indigo was observed. Solvents were then concentrated to ca. 3 mL and the resulting suspension was filtered to give a purple solid, which was washed with portions of pentane (5× 50 mL) and then dried under reduced pressure to give **1a**, as a purple solid. Yield: 2.32 g (79 %); EPR: $g=1.992$, $a_{Mo}=38.8$ G.

Synthesis of $[Mo(C_5H\mathit{i}Pr_4)Cl_4]$ (1b): $PhICl_2$ (6.87 g, 52.50 mmol) dissolved in dichloromethane(20 mL) was added dropwise to a solution of $(C_5H\mathit{i}Pr_4)MoCO_3CH_3$ (6.85 g, 15.98 mmol) in dichloromethane (20 mL). The solution was heated to reflux for 3 h, during which time a color change from brown to indigo was observed. Solvents were then concentrated to about 4 mL and the resulting suspension was filtered. The solid was washed with portions of pentane (5×20 mL) and dried under reduced pressure to give **1b**, as an indigo solid. Yield: 5.27 g (70 %).

Synthesis of $[Mo(1,2,4\text{-}C_5H_2\mathit{t}Bu_3)(PMe_3)_2H_3]$ (2a): Compound **1a** (1415 mg, 3.00 mmol) was dissolved in tetrahydrofuran (20 mL) and a solution of trimethylphosphane in tetrahydrofuran (1 M, 8 mL, 8 mmol) was added. The mixture was stirred for 30 min, and then a suspension of lithium tetrahydroaluminate (ca. 650 mg) in tetrahydrofuran (40 mL) was carefully added. Gas evolution was observed during the addition. The mixture was stirred for 5 h then methanol (ca. 6 mL) was added dropwise causing vigorous gas evolution. The resulting suspension was stirred for 1 h and vacuum-dried; the residue was then extracted with diethyl ether (ca. 150 mL) and filtered through Celite 545. The final solution was vacuum-dried, and the residue washed three times with methanol (6, 4 and 4 mL) and dried in vacuo. The product **2a** was obtained as a pale yellow solid. Yield: 727 mg (50 %); ^{1}H NMR (C_6D_6): $\delta=-5.20$ (t, $J=51.0$ Hz, 3H; Mo-*H*), 1.37 (s, 9H; *t*Bu), 1.49 (br, 18H; P(C*H*$_3$)$_3$), 1.58 (s, 18H; 2*t*Bu), 4.86 ppm (s, 2H; C$_5$*H*$_2$*t*Bu$_3$); ^{31}P{^{1}H} NMR (C_6D_6): δ 17.9 (s); elemental analysis calcd (%) for $C_{23}H_{50}MoP_2$: C 57.01, H 10.40; found: C 56.48, H 10.88. A single crystal for the X-ray analysis was obtained by slow diffusion of a MeOH layer into a solution of **2a** in pentane at 5 °C.

Synthesis of [Mo(C$_5$H*i*Pr$_4$)(PMe$_3$)$_2$H$_3$] (2b): Compound **1b** (890 mg, 1.89 mmol) was dissolved in tetrahydrofuran (20 mL), and a solution of trimethylphosphine in tetrahydrofuran (1 M, 5 mL, 5 mmol) was added. The mixture was stirred for 20 min and a suspension of lithium tetrahydroaluminate (ca. 500 mg) in tetrahydrofuran (40 mL) was carefully added. Gas evolution was observed during the addition. The mixture was stirred for 6 h, after which methanol (ca. 5 mL) was added drop by drop. Vigorous gas evolution was observed at this point. The resulting suspension was stirred for 1 h and then vacuum-dried. The residue was extracted with diethyl ether (ca. 100 mL) and filtered through Celite 545. The final solution was vacuum-dried and the residue washed with portions of methanol (5, 3, and 3 mL) and dried in vacuo. The product **2b** was obtained as an orange-yellow solid. Yield: 449 mg (49 %); ^{1}H NMR (C_6D_6): δ −5.15 (t, $J=52.9$ Hz, 3H; Mo-*H*), 1.30–1.80 (42H; CH(C*H*$_3$)$_2$, P(C*H*$_3$)$_3$), 2.79 (m, 2H; C*H*(CH$_3$)$_2$), 2.96 (m, 2H; C*H*(CH$_3$)$_2$), 4.72 ppm (s, 1H; C$_5$*H**i*Pr$_4$); ^{31}P{^{1}H} NMR (C_6D_6): $\delta=17.3$ ppm (s); elemental analysis calcd (%) for $C_{23}H_{50}MoP_2$: C 57.01, H 10.40; found: C, 56.91; H, 11.10. A single crystal for the X-ray analysis was obtained by diffusion of a MeCN layer onto a solution of **2b** in THF at room temperature.

Synthesis of [Mo(1,2,4-C$_5$H$_2$*t*Bu$_3$)(PMe$_3$)$_2$H$_3$]$^+$PF$_6^-$ (2a$^+$PF$_6^-$): A suspension of [Fe(η^5-C$_5$H$_5$)$_2$]PF$_6$ (32 mg, 0.10 mmol) in tetrahydrofuran (5 mL) was added dropwise to a cold solution (193 K) of compound **2a** (53 mg, 0.11 mmol) in tetrahydrofuran (5 mL). The solution color immediately changed from pale yellow to dark blue and, within a few minutes, to orange. The reaction mixture was slowly warmed up to 253 K and then concentrated to about 1 mL. Addition of cold pentane (253 K, 10 mL) afforded a brown precipitate that was decanted and further washed with cold pentane (253 K, 3x10 mL) and finally vacuum-dried. The product **2a**$^+$PF$_6^-$ was obtained as a pale brown solid. Yield: 48 mg (70 %); EPR (THF): $g=2.0185$, $a_P=36.2$ G, $a_H=11.4$ G, $a_{Mo}=30.8$ G. A single crystal for the X-ray analysis was obtained by diffusion of a pentane layer onto a solution of **2a**$^+$PF$_6^-$ in THF at −80 °C.

Synthesis of [Mo(1,2,4-C$_5$H$_2$*t*Bu$_3$)(PMe$_3$)$_2$H$_4$]$^+$BF$_4^-$ (3a): A solution of **2a** (40 mg, 0.08 mmol) in diethyl ether (4 mL) was cooled to −80 °C. HBF$_4$ (54 % solution in diethyl ether, 22 μL, 0.16 mmol) was added by syringe. Within minutes, a white precipitate formed. A further portion of diethyl ether (2 mL) was added. The solvent was then decanted and the solid washed with portions of diethyl ether (5×3 mL) and dried under reduced pressure to yield **3a** as a white solid. Yield: 39 mg (85 %); ^{1}H NMR ([D$_8$]THF): $\delta=-4.20$ (t, $J=53.4$ Hz, 3H; Mo-H), 1.38 (s, 9H; -*t*Bu), 1.46 (s, 18H; 2*t*Bu), 1.78 (br, 18H; P(C*H*$_3$)$_3$), 5.08 ppm (s, 2H; C$_5$*H*$_2$*t*Bu$_3$); ^{31}P{^{1}H} NMR ([D$_8$]THF): $\delta=0.4$ ppm (s). A single crystal for the X-ray analysis was obtained by diffusion of a diethyl ether layer onto a solution of **3a** in THF at room temperature.

Generation of [Mo(1,2,4-C$_5$H$_2$*t*Bu$_3$)(PMe$_3$)$_2$(MeCN)H$_2$]$^+$BF$_4^-$ (4a): Complex **3a** (10 mg, 0.018 mmol) was measured into an NMR tube and dissolved in CD$_3$CN (0.8 mL). ^{1}H and ^{31}P NMR spectra were recorded initially and again after 5 h. At this time, the resonances corresponding to **3a** were replaced by a new set of resonances, ascribed to **4a**. ^{1}H NMR (CD$_3$CN, 298 K): $\delta=1.07$ (s,9H; C(C*H*$_3$)$_3$), 1.42, (s, 18H; 2×C(C*H*$_3$)$_3$), 1.61 (d, $J=8.7$ Hz, 18H; P(C*H*$_3$)$_3$), 2.17 (s, 3H; CH$_3$CN) 4.59 ppm (m, 2H; C$_5$*H*$_2$*t*Bu$_4$); ^{1}H NMR (CD$_3$CN, 233 K): $\delta=-6.77$ (t, J(P,H)$=40.0$ Hz, 1H; Mo-*H*), −0.27 (t, J(P,H)$=80$ Hz, 1H; Mo-*H*), 1.03 (s, 9H; C(C*H*$_3$)$_3$), 1.38 (s, 18H; C(C*H*$_3$)$_3$), 1.58 (d, J(P,H)$=10$ Hz, 18H; P(C*H*$_3$)$_3$), 2.40 (s, 3H; C*H*$_3$CN), 4.58 ppm (m, 2H; C$_5$*H*$_2$*t*Bu$_3$); ^{31}P{^{1}H} NMR (CD$_3$CN): $\delta=$ 1.85 ppm (s); ^{31}P{^{1}H sel. decoupler at 1.61 ppm}: $\delta=1.88$ ppm (t, $J=52.85$ Hz).

Generation of [Mo(C$_5$H*i*Pr$_4$)(PMe$_3$)$_2$H$_2$(MeCN)]$^+$BF$_4^-$ (4b): A solution of HBF$_4$ (54 % in diethyl ether, 7.4 μL, 0.05 mmol) was added to a solution of **2b** (26 mg, 0.05 mmol) in THF (1 mL) and MeCN (1 mL) at −80 °C. A color change from yellow to orange was observed immediately. Solvents were concentrated to 1 mL and diethyl ether (1 mL) was added to aid the precipitation of a yellow solid. The solution was filtered and the solid washed with portions of diethyl ether (5×2 mL) and dried under reduced pressure to give **4b** as a yellow solid. ^{1}H NMR ([D$_6$]acetone, 298 K): $\delta=-2.5$ (br, 2H; Mo-*H*), 1.18 (d, $J=8.2$ Hz, 12H; CH(C*H*$_3$)$_2$), 1.31, (d, $J=8.6$ Hz, 12H; CH(C*H*$_3$)$_2$), 1.69 (d, $J=9.0$ Hz, 18H; P(C*H*$_3$)$_3$), 2.71 (m, 7H; C*H*(CH$_3$)$_2$, CH$_3$CN) 4.92 ppm (s, 1H; C$_5$*H**i*Pr$_4$); ^{1}H NMR ([D$_6$]acetone, 200 K): $\delta=-5.27$ (td, J(P,H)$=32.5$ Hz, J(H,H)$=10$ Hz 1H; Mo-*H*), −0.13 (ddd, J(P,H)$=47.5$, 33.75, J(H,H)$=$ 10 Hz, 1H; Mo-*H*), 1.07 (d, $J=6.8$ Hz, 3H; CH(C*H*$_3$)$_2$), 1.13 (d, $J=$ 6.8 Hz, 3H; CH(C*H*$_3$)$_2$), 1.18–1.23 (3×d, $J=7.3$, 6.9 Hz, 9H; CH(C*H*$_3$)$_2$), 1.29 (d, $J=7.3$ Hz, 3H; CH(C*H*$_3$)$_2$), 1.39 (2×d, $J=6.5$ Hz, 6H; CH(C*H*$_3$)$_2$), 1.65 (2×d, J(P,H)$=8.0$ Hz, 18H; P(C*H*$_3$)$_3$), 2.53 (m, 1H; C*H*(CH$_3$)$_2$,), 2.58 (m, $J=7.3$ Hz, 1H; C*H*(CH$_3$)$_2$), 2.71 (m, 2H; 2×C*H*(CH$_3$)$_2$), 2.79 (s, 3H; C*H*$_3$CN), 5.02 ppm (d, $J=6$ Hz, 1H; C$_5$*H**i*Pr$_4$); ^{31}P{^{1}H} NMR ([D$_6$]acetone): $\delta=4.66$ ppm (s); ^{31}P{^{1}H sel. decoupler at 1.68 ppm}: $\delta=4.68$ ppm (t, $J=54.7$ Hz).

Formation of [Mo(1,2,4-C$_5$H$_2$*t*Bu$_3$)(PMe$_3$)$_2$H]$^+$PF$_6^-$ (5): A solution of compound **2a**$^+$PF$_6^-$ in THF was stored at −20 °C for 2 days, after which time a mixture of green and dark orange-red crystals had formed. One of the green crystals was used for the X-ray analysis. For the spectroscopic properties, see Results and Discussion.

Single crystal X-ray and neutron diffraction studies: A single crystal of each compound was mounted under inert perfluoropolyether at the tip of glass fiber and cooled in the cryostream of either an Oxford-Diffraction XCALIBUR CCD diffractometer for **2b**, **4a** and **5a** or a Stoe IPDS diffractometer for **2a**, **2a**$^+$. Data were collected using the monochromatic Mo$_{K\alpha}$ radiation ($\lambda=0.71073$). The structures were solved by direct methods (SIR97)[55] and refined by least-squares procedures on F^2 using SHELXL-97.[56] All H atoms attached to carbon were introduced in calculation in idealized positions and treated as riding models. In compound **2a**$^+$, there are two cations and anions in the asymmetric unit and all the *t*Bu groups of one of the cations are disordered over two positions. In structure **2a**, coordinates and U_{iso} for the hydrides were fully refined, whereas in **3a**, the coordinates of the hydrides were fully refined with an overall isotropic thermal parameter. In **2a**$^+$ and **5a**, the coordinates of the hydrides were fully refined with $U_{iso}=1.2\,U_{eq}$[Mo(**2a**$^+$)] or $U_{iso}=1.5\,U_{eq}$[Mo(**5a**)]. The disordered moieties were refined applying the restraints available within SHELXL97.[56] Moreover, some residual electron density was difficult to model and therefore, the SQUEEZE function of PLATON[57] was used to eliminate the contribution of the electron density in the solvent region from the intensity data, and the solvent-free model was employed for the final refinement. There are four cavities per unit cell and PLATON estimated that each cavity contains 32 electrons which could be attributed to a disordered THF molecules. The data collected for compound **2b** were of very low quality and although the structural model is mainly correct, it was not possible to locate any hydride ligand. The drawing of the molecules was realized with the help of ORTEP32.[58] Crystal data and refinement parameters are shown in Table 2.

The neutron single-crystal diffraction study was performed using the time-of-flight Laue diffractometer SXD[59] installed at the ISIS pulsed spallation source. SXD uses the white beam Laue technique and a stationary crystal combined with eleven highly pixellated area detectors covering around half a sphere around the sample. Thus, large volumes in reciprocal space can be collected in a single shot. A suitable single crystal of the complex (**2a**) was fixed to an Aluminum pin with thin strips of adhesive Al tape and mounted on a He closed-cycle refrigerator and cooled slowly to 20 K. The space group $P2_1/n$ was confirmed at 20 K. No significant change in the crystal mosaic or splitting of the peak was observed during cooling. Further crystallographic data and experimental details are given in Table 2 and in the Supporting Information. The unit cell di-

Table 2. Crystal data and structure refinement for all structurally characterized complexes.

	2a (X-ray)	**2a** (neutron)	**2b**	**3a**	**2a**$^+$	**5a**
formula	$C_{23}H_{50}MoP_2$	$C_{23}H_{50}MoP_2$	$C_{23}H_{50}MoP_2$	$C_{23}H_{51}BF_4MoP_2$	$C_{23}H_{50}F_6MoP_3$	$C_{23}H_{48}F_6MoP_3$
M_r	484.51	484.51	481.49	572.33	629.48	627.46
T [K]	180(2)	20(1)	180(2)	180(2)	180(2)	180(2)
crystal system	monoclinic	monoclinic	monoclinic	monoclinic	monoclinic	monoclinic
space group	$P2_1/n$	$P2_1/n$	$P2_1/c$	$P2_1/c$	$P2_1/c$	$P2_1/c$
a [Å]	16.2915(15)	16.238(5)	15.599(4)	9.3986(5)	14.0847(10)	9.6185(5)
b [Å]	17.4655(16)	17.392(5)	10.2114(18)	16.9428(8)	26.216(2)	16.8699(10)
c [Å]	9.2144(8)	9.160(4)	16.939(4)	18.2340(9)	20.1855(15)	18.7489(12)
α [°]	90.0	90.0	90.0	90.0	90.0	90.0
β [°]	92.651(10)	92.83(1)	103.51(2)	92.719(4)	99.221(8)	90.441(5)
γ [°]	90.0	90.0	90.0	90.0	90.0	90.0
V [Å^3]	2619.1(4)	2584(2)	2623.5(10)	2900.3(3)	7357.2(10)	3042.2(3)
Z	4	4	4	4	8	4
ρ_{calcd} [Mg m^{-3}]	1.229	1.246	1.227	1.311	1.269	1.370
μ [mm^{-1}]	0.629	$0.0655+0.0002\lambda$	0.628	0.597	0.535	0.636
crystal size [mm^3]	$0.27\times0.23\times0.2$	$2.2\times1.6\times1.4$	$0.13\times0.1\times0.1$	$0.25\times0.21\times0.13$	$0.2\times0.1\times0.1$	$0.58\times0.42\times0.24$
θ range [°]	2.49–26.18	8.52–81.95	3.17–23.20	2.76–28.22	2.14–25.00	3.25–26.37
reflns collected	20750	8686	14396	24326	50093	27114
independent reflns [Rint]	5171 [0.0337]	3203 [0.141]	3766 [0.1239]	7190 [0.0392]	12934 [0.0853]	18993 [0.0513]
absorption correction	Multi-scan	Gaussian	Multi-scan	Multi-scan	Multi-scan	Multi-scan
max/min transmission	0.8299, 0.7768	1.5609, 1.626	1.0214, 0.8735	0.9996, 0.8209	0.8843, 0.8674	0.8363, 0.7206
data/restraints/parameters	5171/0/262	3203/0/686	3766/204/249	7190/0/308	12934/216/763	18993/0/317
GOF on F^2	1.034	1.023	1.129	1.013	0.835	1.070
$R1$, $wR2$ [$I>2\sigma(I)$]	0.0270, 0.0657	0.0603, 0.1542	0.1029, 0.2176	0.0333, 0.0788	0.0488, 0.1052	0.0507, 0.1428
$R1$, $wR2$ (all data)	0.0357, 0.0708	0.0608, 0.1546	0.1592, 0.2396	0.0508, 0.0901	0.0963, 0.1174	0.0599, 0.1554

mensions were precisely calculated, at the end of the data collection, from the positions of 60 reflections per each detector orientation. Data were collected at nine different orientations at 20(1) K for approximately 24 h per orientation. The range of wavelengths used for the data collection was $0.37<\lambda<8.8$ Å, even though the bulk of the diffraction information is obtained from the wavelength range $0.5<\lambda<7.0$ Å. Data reduction and a Gaussian absorption correction were performed using the standard SXD procedure implemented in the SXD2001 software[60] resulting in a total of 8686 reflections of which 3203 were unique. The starting structural model for the refinement was based on the atomic coordinates for the non hydrogen atoms taken from the X-ray structural determination. The structure was refined by full-matrix least-squares methods, with a minimizing the function $[\Sigma w(F_o^2-(1/k)F_c^2)^2]$ and by using all independent data. During the refinement, the difference-Fourier maps clearly showed all hydrogen atoms of the ligands and the three hydrides. The final structure model included coordinates and anisotropic displacement parameters for all atoms. Upon convergence the final Fourier difference map showed no significant features. The coherent scattering amplitudes used were those tabulated by Rauch and Waschkowski.[61] All calculations were carried out by using the PC version of the programs WINGX,[62] SHELX-97,[56] and ORTEP.[58]

CCDC-631893–631898 contains the supplementary crystallographic data for this paper. These data can be obtained free of charge from The Cambridge Crystallographic Data Centre via www.ccdc.cam.ac.uk/data_request/cif.

Acknowledgements

We thank the European Commission through the HYDROCHEM program (contract HPRN-CT-2002-00176) for support of this work. M.B. thanks the Spanish Ministerio de Educación y Ciencia for a postdoctoral fellowship.

---

[1] G. W. Parshall, *Homogeneous Catalysis: The Applications and Chemistry of Catalysis by Soluble Transition Metal Complexes*, Wiley, New York, **1980**.

[2] A. Dedieu, *Transition Metal Hydrides*, VCH, Weinheim, **1992**.

[3] M. Peruzzini, R. Poli, *Recent Advances in Hydride Chemistry*, Elsevier, Amsterdam, **2001**.

[4] R. Y. Igarashi, M. Laryukhin, P. C. Dos Santos, H.-I. Lee, D. R. Dean, L. C. Seefeldt, B. M. Hoffman, *J. Am. Chem. Soc.* **2005**, *127*, 6231–6241.

[5] S. Foerster, M. Stein, M. Brecht, H. Ogata, Y. Higuchi, W. Lubitz, *J. Am. Chem. Soc.* **2003**, *125*, 83–93.

[6] R. Mejia-Rodriguez, D. S. Chong, J. H. Reibenspies, M. P. Soriaga, M. Y. Darensbourg, *J. Am. Chem. Soc.* **2004**, *126*, 12004–12014.

[7] O. B. Ryan, M. Tilset, V. D. Parker, *J. Am. Chem. Soc.* **1990**, *112*, 2618–2626.

[8] K.-T. Smith, C. Rømming, M. Tilset, *J. Am. Chem. Soc.* **1993**, *115*, 8681–8689.

[9] B. Pleune, D. Morales, R. Meunier-Prest, P. Richard, E. Collange, J. C. Fettinger, R. Poli, *J. Am. Chem. Soc.* **1999**, *121*, 2209–2225.

[10] V. Skagestad, M. Tilset, *J. Am. Chem. Soc.* **1993**, *115*, 5077–5083.

[11] R. Poli, in *Recent Advances in Hydride Chemistry* (Eds.: R. Poli, M. Peruzzini), Elsevier Science, Amsterdam, **2001**, pp. 139–188.

[12] B. Pleune, R. Poli, J. C. Fettinger, *J. Am. Chem. Soc.* **1998**, *120*, 3257–3258.

[13] E. A. Quadrelli, H.-B. Kraatz, R. Poli, *Inorg. Chem.* **1996**, *35*, 5154–5162.

[14] J. C. Fettinger, H.-B. Kraatz, R. Poli, E. A. Quadrelli, R. C. Torralba, *Organometallics* **1998**, *17*, 5767–5775.

[15] E. A. Quadrelli, R. Poli, *Organometallics* **1998**, *17*, 5776–5781.

[16] R. Poli, M. Baya, R. Meunier-Prest, S. Raveau, *New J. Chem.* **2006**, *30*, 759–773.

[17] A. A. Zlota, M. Tilset, K. G. Caulton, *Inorg. Chem.* **1993**, *32*, 3816–3821.

[18] A. Pedersen, M. Tilset, *Organometallics* **1994**, *13*, 4887–4894.

[19] M. T. Costello, R. A. Walton, *Inorg. Chem.* **1988**, *27*, 2563–2564.

[20] K.-T. Smith, M. Tilset, R. Kuhlman, K. G. Caulton, *J. Am. Chem. Soc.* **1995**, *117*, 9473–9480.

[21] M. Baya, J. Houghton, J.-C. Daran, R. Poli, *Angew. Chem.* **2007**, *119*, 433–436; *Angew. Chem. Int. Ed.* **2007**, *46*, 429–432.

[22] R. C. Murray, L. Blum, A. H. Liu, R. R. Schrock, *Organometallics* **1985**, *4*, 953–954.

[23] D. W. Keogh, R. Poli, in *Synthetic Methods of Organometallic and Inorganic Chemistry (Herrmann/Brauer), Vol. 8* (Ed.: W. A. Herrmann), Thieme, Stuttgart, **1997**, p. 98.

[24] J. H. Shin, G. Parkin, *Chem. Commun.* **1998**, 1273–1274.

[25] J. C. Fettinger, B. Pleune, R. Poli, *J. Am. Chem. Soc.* **1996**, *118*, 4906–4907.

[26] B. Pleune, R. Poli, J. C. Fettinger, *Organometallics* **1997**, *16*, 1581–1594.

[27] H. Sakaba, T. Hirata, C. Kabuto, K. Kabuto, *Organometallics* **2006**, *25*, 5145–5150.

[28] G. J. Kubas, *Metal Dihydrogen and σ-Bond Complexes*, Kluwer/Press, New York, **2001**.

[29] D. M. Heinekey, J. M. Millar, T. F. Koetzle, N. G. Payne, K. W. Zilm, *J. Am. Chem. Soc.* **1990**, *112*, 909–919.

[30] J. A. K. Howard, O. Johnson, T. F. Koetzle, J. L. Spencer, *Inorg. Chem.* **1987**, *26*, 2930–2933.

[31] J. A. K. Howard, S. A. Mason, O. Johnson, I. C. Diamond, S. Crennell, P. A. Keller, J. L. Spencer, *J. Chem. Soc. Chem. Commun.* **1988**, 1502–1503.

[32] L. Brammer, J. A. K. Howard, O. Johnson, T. F. Koetzle, J. L. Spencer, A. M. Stringer, *J. Chem. Soc. Chem. Commun.* **1991**, 241–243.

[33] T. Hasegawa, Z. Li, S. Parkin, H. Hope, R. K. McMullan, T. F. Koetzle, H. Taube, *J. Am. Chem. Soc.* **1994**, *116*, 4352–4356.

[34] T. J. Johnson, A. Albinati, T. F. Koetzle, J. Ricci, O. Eisenstein, J. C. Huffman, K. G. Caulton, *Inorg. Chem.* **1994**, *33*, 4966–4976.

[35] T. M. Cameron, C. G. Ortiz, I. Ghiviriga, K. A. Abboud, J. M. Boncella, *J. Am. Chem. Soc.* **2002**, *124*, 922–923.

[36] R. Poli, *Organometallics* **1990**, *9*, 1892–1900.

[37] F. Abugideiri, J. C. Fettinger, D. W. Keogh, R. Poli, *Organometallics* **1996**, *15*, 4407–4416.

[38] T.-Y. Cheng, D. J. Szalda, J. Zhang, R. M. Bullock, *Inorg. Chem.* **2006**, *45*, 4712–4720.

[39] D. M. Heinekey, A. Lledós, J. M. Lluch, *Chem. Soc. Rev.* **2004**, *33*, 175–182.

[40] J. Sandström, *Dynamic NMR Spectroscopy*, Academic Press, London, **1982**.

[41] G. Binsch, *J. Am. Chem. Soc.* **1969**, *91*, 1304–1309.

[42] R. Poli, *Chem. Rev.* **1996**, *96*, 2135–2204.

[43] R. Poli, *J. Organomet. Chem.* **2004**, *689*, 4291–4304.

[44] D. G. Morrell, J. K. Kochi, *J. Am. Chem. Soc.* **1975**, *97*, 7262–7270.

[45] T. T. Tsou, J. K. Kochi, *J. Am. Chem. Soc.* **1978**, *100*, 1634–1635.

[46] W. Lau, J. C. Huffman, J. K. Kochi, *Organometallics* **1982**, *1*, 155–169.

[47] A. Pedersen, M. Tilset, *Organometallics* **1993**, *12*, 56–64.

[48] P. Diversi, S. Iacoponi, G. Ingrosso, F. Laschi, A. Lucherini, C. Pinzino, G. Uccello-Barretta, P. Zanello, *Organometallics* **1995**, *14*, 3275–3287.

[49] E. Fooladi, M. Tilset, *Inorg. Chem.* **1997**, *36*, 6021–6027.

[50] E. Fooladi, T. Graham, M. L. Turner, B. Dalhus, P. M. Maitlis, M. Tilset, *J. Chem. Soc. Dalton Trans.* **2002**, 975–982.

[51] H. Sitzmann, *J. Organomet. Chem.* **1988**, *354*, 203–214.

[52] H. Sitzmann, *Z. Naturforsch. B* **1989**, *44*, 1293–1297.

[53] K. Marat, *SpinWorks Version 2.5.4*, **2006**.

[54] D. R. Duling, P.E.S.T., v. 0.96, National Institute of Environmental Health Sciences, Research Triangle Park, NC, **1996**.

[55] A. Altomare, M. Burla, M. Camalli, G. Cascarano, C. Giacovazzo, A. Guagliardi, A. Moliterni, G. Polidori, R. Spagna, *J. Appl. Crystallogr.* **1999**, *32*, 115–119.

[56] G. M. Sheldrick, SHELXL97, Program for Crystal Structure Refinement, University of Göttingen, Göttingen, Germany, **1997**.

[57] A. L. Spek, *J. Appl. Crystallogr.* **2003**, *36*, 7–13.

[58] L. J. Farrugia, *J. Appl. Crystallogr.* **1997**, *30*, 565.

[59] D. A. Keen, M. J. Gutmann, C. C. Wilson, *J. Appl. Crystallogr.* **2006**, *39*, 714.

[60] M. J. Gutmann, ISIS Facility, Rutherford Appleton Laboratory, U. K., **2006**.

[61] H. Rauch, W. Waschkowski, in *Neutron Data Booklet* (Eds.: A. J. Dianoux, G. Lander), Institut Laue-Langevin: Grenoble, **2002**, pp. 1.1–1.

[62] L. J. Farrugia, *J. Appl. Crystallogr.* **1999**, *32*, 837–838.

Received: February 21, 2007